Intensification of Near-Inertial Currents in the Atlantic Ocean Over the Past Two Decades

Yuhang Zheng[1,2,3,4], Xiaoming Zhai[2], David P. Stevens[5], Wei Wu[1,3,6], Wenhao Gong[1,3,4], Yan Du[1,3,4*]

1. State Key Laboratory of Tropical Oceanography, South China Sea Institute of Oceanology, Chinese Academy of Sciences, Guangzhou, China
2. Centre for Ocean and Atmospheric Sciences, School of Environmental Sciences, University of East Anglia, Norwich, UK
3. Guangdong Key Laboratory of Ocean Remote Sensing and Big Data, Guangzhou, China
4. University of Chinese Academy of Sciences, Beijing, China
5. Centre for Ocean and Atmospheric Sciences, School of Engineering, Mathematics and Physics, University of East Anglia, Norwich, UK
6. Ocean and Earth Science, University of Southampton, Southampton, UK

Final version for Nature Communications

Corresponding author*:

Yan Du (duyan@scsio.ac.cn)

Abstract

Near-inertial currents (NICs) play a key role in surface material redistribution and ocean mixing, yet their long-term variability remains poorly known. Using in situ current measurements from surface drifters, we provide observational evidence for a pronounced intensification of surface NICs in the Atlantic Ocean over the past two decades (2003–2022). Basin–mean NIC strength increases at a rate of 3.8 ± 1.7% per decade, with a spatial pattern characterized by strengthening in the South Atlantic and the high-latitude North Atlantic, and weakening in the low-latitude North Atlantic. We further show that these trends in Atlantic NICs are primarily driven by changes in near-inertial wind forcing, particularly those associated with mesoscale weather systems, while variations in mixed-layer depth playing a minor role. This observed intensification of Atlantic NICs may have important implications for ocean transport and mixing, and needs to be properly represented in the current generation of climate models.

Introduction

As a core component of the Earth's climate system, ocean currents play a fundamental role in regulating global climate and sustaining marine ecosystems by mediating the multiscale transport of heat, carbon, and nutrients[1-5]. Depending on their characteristic temporal and spatial scales and underlying dynamical mechanisms, ocean currents can be broadly decomposed into several components, including ocean gyre circulation, mesoscale eddies, sub-mesoscale motions, Ekman flows, tides, and near-inertial currents (NICs). Among these components, NICs stand out as one of the most energetic high-frequency motions, oscillating at frequencies close to the local inertial frequency[6-9]. They are tightly coupled to atmospheric variability and derive the majority of their energy from wind forcing, with near-inertial wind power estimates ranging from 0.26 to 1.4TW depending on the wind products and methods used[10-17]. In the surface ocean, NICs play an essential role in shaping the transport pathways of floating materials, often producing arc-shaped, semi-circular, near-circular, or flower-like trajectories that strongly influence drift prediction, pollutant dispersion, and marine search-and-rescue operations[18-20]. Globally, approximately 1/3 of the lifetime of surface-floating objects featured clear near-inertial trajectories[20]. In addition, near-inertial oscillations within the mixed layer can radiate as downward-propagating near-inertial internal waves, providing a major conduit for transferring wind energy from the surface boundary layer into the ocean interior. This downward energy flux constitutes a key energy source for deep-ocean mixing and thereby contributes to the maintenance of the global overturning circulation[9,21-25].

Under ongoing global warming, multiple components of the ocean currents have already exhibited pronounced long-term changes[26-33]. For example, western boundary currents have undergone significant intensification as well as poleward and shoreward shifts[26,32], mesoscale eddy kinetic energy has strengthened across large portions of the global upper ocean[28], and both the generation and propagation speeds of internal tides have increased markedly[31,33]. In contrast, despite their climatic and dynamical importance, long-term changes in NICs remain poorly constrained. Due to their high-frequency nature, observational coverage of these signals is limited, and they are often filtered out from both observations and the atmospheric forcing used in ocean models. An early study using NCEP reanalysis winds to drive a slab model revealed an approximately 25% increase in global near-inertial wind power from 1948 to 2001[12]. More recent studies employing slab-model or MITgcm simulations forced by ERA5 reanalysis wind products have also suggested significant increases in near-inertial wind power input and near-inertial energy associated with tropical cyclones and over the Southern Ocean[34,35]. However, these model-based estimates are subject to model biases and deficiencies and remain largely unvalidated against in situ ocean measurements, leaving the magnitude and robustness of long-term NIC changes in the real ocean uncertain.

Here, we address this gap by leveraging the global surface drifters to directly quantify changes in upper-ocean NICs. A gridded and significance-testing framework is developed to enable robust estimation of regional NIC trends from spatially sparse

drifter observations, providing a systematic assessment of NIC variability over the period 2003–2022. The results indicate that upper-ocean NICs have strengthened across most of the global ocean, with the Atlantic exhibiting the most pronounced and spatially-coherent change (**Fig. 1b, d**). Owing to its dense drifter sampling (**Supplementary Fig. 1**) and the strong, latitudinally coherent signal in its NIC trends, the Atlantic is selected as the primary basin of focus. Analyses based on two state-of-the-art reanalysis hourly wind products (ERA5 and CFS) show that changes in near-inertial wind forcing largely account for the observed NIC trends in the Atlantic. In addition, slab-model experiments reveal that long-term variations in mixed-layer depth (MLD) further modulate the NIC response. Collectively, these findings provide an observation-based attribution of long-term changes in Atlantic NICs and establish a reliable foundation for future observational and modelling studies of near-inertial motions.

Results

Observed Intensification of Near-Inertial Currents

By applying a band-pass filter to the global surface drifter velocity records (see Methods), we extracted near-inertial speed at each drifter location and aggregated them onto a 2° × 2° grid to compute long-term mean fields (**Fig. 1a**). The resulting climatology shows that NICs are strongest in the mid-latitude westerly wind regions of both hemispheres, with amplitudes exceeding 10 cm s^{-1}. The zonal-mean distribution reveals a clear latitudinal dependence, with NIC speed increasing with latitude and peaking near 40°. Histogram-based basin-scale averages indicate a global mean NIC speed of 7.5±2.8 cm s^{-1}, with relatively similar distributions among the major ocean basins (**Fig. 1c**). When examined by latitude bands, the Northern Hemisphere high latitudes (30–60°N) exhibit the strongest NICs, with a mean value of 10.4±2.7 cm s^{-1}, followed by the Southern Hemisphere high latitudes (30–60°S). In contrast, lower-latitude regions in both hemispheres (5–30°N and 5–30°S) show substantially weaker NICs, highlighting a pronounced meridional inhomogeneity in near-inertial energy distribution.

Because the number of available drifters increased substantially only after 2003 (**Supplementary Fig. 1a**), we evaluated linear trends in NIC speed over the period 2003–2022 and mapped them onto the same 2° × 2° grid (**Fig. 1b**). Grid points with insufficient data coverage or statistically insignificant trends are shown in white (see Methods). Because kinetic energy depends quadratically on speed, it is more sensitive to the spatially discrete drifter sampling. We therefore focus on the more robustly estimated trends in NIC speed. The resulting trend map exhibits alternating positive and negative signals across different regions, likely reflecting genuine variability in NICs, and possibly the influence of the spatially heterogeneous distribution of drifter observations. On the global average, NIC speed increases at a rate of 2.1 ± 1.0% per decade. Basin-mean trends indicate increases by 3.8 ± 1.7% per decade in the Atlantic Ocean, 1.5 ± 0.8% per decade in the Pacific Ocean, 1.2 ± 0.8% per decade in the Indian Ocean, and 2.1 ± 1.1% per decade in the Southern Ocean (**Fig. 1d**).

Notably, the Atlantic Ocean exhibits the most pronounced and spatially-coherent signals (**Fig. 1b**). Given that the Atlantic also has the densest drifter coverage among all basins (**Supplementary Fig. 1b**), whereas other basins show basin-mean increases without spatially consistent patterns in the gridded fields, subsequent analyses focus primarily on the Atlantic Ocean. Latitudinally, the strongest increase is observed in the high-latitude North Atlantic (NA), with a trend of 7.6 ± 2.4% per decade. Significant increases are also found in the low-latitude South Atlantic (SA) and high-latitude SA, with trends of 3.4 ± 1.8% and 5.0 ± 2.0% per decade, respectively. In contrast, the low-latitude NA exhibits a marked weakening trend of −3.6 ± 0.7% per decade (**Fig. 1d**).

Monthly analyses indicate that changes in NIC speed in the Atlantic Ocean are broadly uniform throughout the year, with only slightly weaker increasing trends during boreal summer (**Supplementary Fig. 2**). Moreover, all seasons consistently exhibit strengthening NICs in the high-latitude NA as well as in the SA, while a weakening signal persists in the low-latitude NA. These results demonstrate that the observed intensification in Atlantic NICs occurs year-round, rather than being confined to a particular season.

Role of Wind Forcing

Because NICs in the ocean are primarily driven by wind forcing, we examined whether the observed changes in near-inertial speed are associated with corresponding changes in the wind field. To this end, we employed two state-of-the-art reanalysis wind products with hourly resolution to quantify near-inertial wind stress (NIWS), which is known to be most efficient at exciting NICs through inertial resonance[7,34,36]. **Figure 2** presents the climatological mean state and linear trends of Atlantic NIWS calculated solely from gridded wind fields, without accounting for ocean surface currents in the stress calculation. Both wind products reveal a pronounced meridional structure, with NIWS decreasing from high to low latitudes and attaining values at high latitudes that are approximately two to three times larger than those in low-latitude regions (**Fig. 2a, b, e**). NIWS derived from the CFS wind product is consistently larger than that from ERA5 across all latitude bands. The spatial pattern of the mean NIWS closely resembles that of NIC speed, indicating a strong link between wind forcing and the distribution of upper-ocean NICs. Consistent with this spatial agreement, NIWS trends over the past two decades also mirror the observed changes in NICs (**Fig. 2c, d**). Both wind products indicate a significant basin-wide increase in Atlantic NIWS, with trend magnitudes of 2.7 ± 1.9% per decade and 4.6 ± 1.9% per decade derived from ERA5 and CFS, respectively (**Fig. 2f**). In addition, both datasets show pronounced increases in NIWS in the SA and high-latitude NA, accompanied by a clear decrease in the low-latitude NA. With the exception of low-latitude NA, where the two products yield comparable results, the magnitudes of both positive and negative trends derived from CFS are systematically larger than those from ERA5.

We further computed NIWS using an alternative formulation that accounts for surface ocean velocities in the wind stress calculation (see Methods; **Supplementary Fig. 3**). The resulting spatial patterns are broadly consistent with those shown in **Fig. 2**. In terms of trends, increases and decreases are generally stronger than those obtained

using the wind-only formulation, except in the low-latitude SA. This leads to basin-mean Atlantic NIWS trends slightly higher than those calculated solely from gridded wind fields. Results from both stress calculation approaches and two wind products consistently reveal a pronounced increase in NIWS, with magnitudes comparable to those of NIC changes. This close correspondence suggests that NIWS represents a key driver of the observed changes in NICs over the past two decades.

In addition to NIWS, we quantified near-inertial wind power (NIWP), the rate at which wind directly injects energy into oceanic near-inertial motions. The spatial pattern of mean NIWP broadly resembles those of NIWS and NIC speed, but exhibits a more pronounced contrast across latitude bands (**Fig. 3a, b**). Both wind products indicate that NIWP attains its largest values in the high-latitude SA, reaching 1.20 and 1.26 mW m^{-2} based on ERA5 and CFS, respectively (**Fig. 3e**). The second-largest values occur in the high-latitude NA, with NIWP of 0.94 and 1.02 mW m^{-2} derived from ERA5 and CFS, respectively. In both regions, mean NIWP values are substantially larger than those in low-latitude areas. This enhanced latitudinal contrast arises from the fact that NIWP scales with the product of NIWS and NIC speed, thereby amplifying regional differences relative to those seen in NIWS or NICs alone. The temporal evolution of NIWP mirrors the pattern observed for NIC speed (**Fig. 3c, d**). On a basin-wide average, Atlantic NIWP increases at rates of 8.3% per decade and 14.1% per decade based on ERA5 and CFS, respectively (**Fig. 3f**). Regionally, significant increases are evident in the high-latitude NA and in the SA, while a marked decrease is observed in the low-latitude NA. Together, these results show consistent changes in NIWS, wind-to-ocean near-inertial energy input, and NICs in the Atlantic over the past two decades. The strong spatial correspondence among NIWS, NIWP, and NIC further supports the important role of wind forcing in regulating NICs (**Supplementary Fig. 4**).

To assess what atmospheric processes are responsible for the observed changes in NIWS and NIWP, we further analyzed the rotary power spectra of Atlantic wind speed and their trends over the past two decades (**Fig. 4**). The climatological wind power spectra derived from both datasets exhibit consistent patterns. Across all latitudes, wind energy is concentrated at periods shorter than 8 days. Moreover, with increasing latitude, the high-energy region progressively extends toward higher-frequency bands (**Fig. 4a, b**). Unlike ocean current spectra, wind power spectra do not exhibit a pronounced peak at near-inertial frequencies. Nevertheless, significant temporal changes in wind energy within the near-inertial band have also emerged over the past two decades (**Fig. 4c, d**). Specifically, wind energy in the high-latitude NA has intensified at periods of 13 hour–6 day. In contrast, the low-latitude NA exhibits a general decline in wind energy over periods of 13 hour–10 day. In the SA, CFS data indicate an increase in wind variability at periods of 13 hour–2 day, whereas ERA5 shows alternating positive and negative trends over 13 hour–4 day, with localized regions exhibiting increases within the near-inertial band. These changes in near-inertial wind energy closely correspond to the observed changes in NIWS and NICs.

Previous studies have shown that NIWS is primarily influenced by two classes of atmospheric processes: synoptic weather systems and mesoscale weather systems, with

characteristic time scales of 2–6 days and 1 hour–2 days, respectively [34,37]. Our power spectral analysis indeed reveals that changes in wind energy within the near-inertial band closely align with variability associated with these two atmospheric processes. To distinguish their respective contributions, we further examined the kinetic energy trend associated with wind fluctuations over 1 hour–2 day and 2–6 day periods (**Supplementary Fig. 5**). The results show that changes in Atlantic near-inertial wind energy are strongly aligned with variations in mesoscale weather systems, whereas they differ markedly from those associated with synoptic weather systems, and even exhibit opposite trends in the high-latitude SA and parts of the high-latitude NA. We further assess their interannual correlations with near-inertial wind energy (**Supplementary Fig. 6**). Mesoscale weather systems exhibit significant positive correlations across nearly all regions, including near-equatorial areas where the local inertial period exceeds 2 days. In contrast, synoptic weather systems show positive correlations primarily in low-latitude regions below 30°, with substantially weaker magnitudes than those associated with mesoscale systems. At higher latitudes, synoptic variability displays limited positive correlations and is instead characterized by widespread significant negative correlations. Taken together, these findings suggest that mesoscale weather systems are likely the dominant atmospheric processes driving the observed changes in near-inertial wind energy, NIWS, and NICs in the whole Atlantic over the past two decades, whereas synoptic weather systems exert a more limited influence, primarily confined to low-latitude regions.

Role of Mixed-layer depth

Wind-driven near-inertial energy at the ocean surface is generally considered to be distributed within the mixed layer, such that MLD represents an important factor modulating surface NICs[9,17,34]. For a given amount of near-inertial energy input, a deeper mixed layer leads to weaker near-inertial speed within the mixed layer. To quantify the contribution of MLD changes to the observed evolution of Atlantic NIC speed over the past two decades, we conducted a set of controlled experiments using a slab model driven by the two wind products, ERA5 and CFS. We conduct paired simulations with identical wind forcing but different MLD fields: one uses the climatological monthly mean MLD, retaining only the seasonal cycle, while the other uses the observed monthly MLD, including both seasonal and long-term variability.

The slab model broadly reproduces the observed evolution of Atlantic NIC speed, yielding spatial patterns that are comparable to those derived from drifter observations (**Fig. 5a-d**). Although the simulated rates of increase are lower than those inferred from observations (**Fig. 5e**), likely because the slab model assumes a vertically uniform mixed-layer velocity and highly idealized damping and downward energy radiation processes[17,38], it remains well suited for isolating and quantifying the relative contribution of long-term MLD changes to the observed changes in NICs. When the climatological MLD is used, the slab model driven by ERA5 and CFS winds yields Atlantic NIC speed increases of 1.3 ± 0.6% and 2.7 ± 1.0% per decade, respectively. When the observed monthly MLD is prescribed, these rates increase to 1.4 ± 0.8% and 2.9 ± 0.7% per decade, suggesting a modest positive contribution of MLD changes to

the basin-scale increase in Atlantic NIC speed. However, this contribution is unlikely to be significant, as the uncertainty ranges overlap. Regionally, the impact of MLD changes differs between high-latitude and low-latitude Atlantic regions. In slab model simulations using the observed monthly MLD, the increasing trends at high latitudes decrease modestly for both wind products, although the changes are unlikely to be significant. In contrast, the trends at low latitudes shift significantly toward more positive values. For example, in the CFS-driven simulation, the near-inertial speed trend in the low latitude SA changes from −1.8 ± 0.5% per decade when climatological monthly MLD is used to 1.5 ± 0.6% per decade when the observed monthly MLD is prescribed, bringing the simulated trend closer to observations. Sensitivity tests further indicate that neither the specific MLD estimation method (**Supplementary Fig. 7**) nor the choice of the damping parameter r (**Supplementary Fig. 8**) in the slab model exerts a substantial influence on these results.

Overall, long-term MLD changes exert a negative contribution to the growth of NICs in the high-latitude Atlantic and a positive contribution in low-latitude regions. When integrated over the entire basin, MLD changes result in a minor and insignificant net positive contribution to the increase in Atlantic NIC speed, further supporting the dominant role of long-term wind-field changes in the observed NIC intensification.

Discussion

Using in situ surface drifter observations, we show that NICs in the Atlantic Ocean have intensified over the period 2003–2022, at a rate of 3.8 ± 1.7% per decade. Regionally, the strongest increase occurs in the high-latitude NA, reaching 7.6 ± 2.4% per decade. Significant increases are also observed in the low- and high-latitude SA, with trends of 3.4 ± 1.8% and 5.0 ± 2.0% per decade, respectively. In contrast, the low-latitude NA displays a weakening trend of −3.6 ± 0.7% per decade. Consistent changes in NIWS and NIWP derived from both ERA5 and CFS winds closely match the spatial patterns and magnitudes of NIC changes, providing strong evidence that changes in wind forcing are the primary driver of the observed trends in Atlantic NICs. Further analysis of wind rotary power spectra suggests that mesoscale weather systems are likely the dominant atmospheric processes driving the observed changes in near-inertial wind energy, NIWS, and the associated evolution of NICs in the Atlantic. In addition, slab-model experiments indicate that changes in MLD also modulate NIC speed, yielding a minor and insignificant net positive contribution over the entire Atlantic basin.

A key remaining question is whether the observed intensification of NICs reflects decadal variability or a longer-term trend under global warming. Although surface drifter observations become sufficiently dense only over the past two decades, the ERA5 reanalysis provides continuous wind records spanning several decades. Given the strong correlation between near-inertial currents and NIWS in both their spatial distributions and trends, we use the NIWS time series derived from ERA5 winds over 1961–2022 as a proxy for long-term changes in surface NIC speed (**Fig. 6**). The results reveal a significant long-term increase in Atlantic NIWS since 1961, at a rate of

approximately 1.4 ± 0.2% per decade, slightly weaker than the 1.5 ± 0.9% per decade increase observed over the past two decades. Regionally, NIWS exhibits significant long-term increases across all Atlantic subregions since 1961. In the high-latitude North Atlantic and both the low- and high-latitude South Atlantic, the trends over the recent two decades are comparable to or exceed their corresponding long-term trends. By contrast, the recent trend in the low-latitude North Atlantic reverses sign, indicating a decrease that may partly reflect decadal variability in tropical cyclones and low-latitude storms, which has been suggested to be influenced by the Atlantic Multidecadal Variability[39]. Together, these findings indicate that the observed increase in Atlantic NIC speed is likely a manifestation of long-term changes in the wind field associated with global warming, while the pronounced weakening in the low-latitude North Atlantic may reflect superimposed decadal variability acting on this background trend. Consistent with this interpretation, the global analysis shows that NIWS exhibits a comparable increase over both the past six and the past two decades (**Fig. 6f**). This long-term intensification of near-inertial wind forcing is consistent with the earlier finding that reported an approximately 25% increase in global near-inertial wind power over 1948–2001[12]. Together, these results suggest that the observed global enhancement of NICs may partly reflect long-term changes in wind forcing under a warming climate.

This study provides an assessment of long-term trends in ocean surface currents derived directly from in situ current measurements. Our analysis demonstrates that the density of surface drifter observations has become sufficient over the past two decades to quantify changes in NICs, offering an important benchmark for future studies of ocean current variability. Given that most contemporary assessments of ocean circulation rely on geostrophic currents inferred from sea surface height, temperature, and salinity fields, surface drifters provide a unique and complementary perspective by directly capturing ageostrophic and high-frequency motions. This highlights the need for continued and expanded deployment of surface drifters to better support future observational studies. With the continued expansion of the global drifter array, in situ current observations are expected to play an increasingly important role in characterizing multiscale changes in ocean currents.

Owing to the spatially discrete distribution of surface drifters, direct estimation of kinetic energy trends introduces substantially larger sampling-related uncertainties than estimates based on velocity, because kinetic energy scales with the square of velocity. We therefore focus on trends in NIC speed, which can be more robustly quantified from available observations. This quadratic dependence implies that the observed increase in NIC speed corresponds to an even stronger enhancement of near-inertial energy. Consistent with this interpretation, NIWP, which quantifies wind-driven energy input into near-inertial motions, indicates an Atlantic near-inertial energy increase of approximately 8.3–14.1% per decade. When placed in the context of previously reported global mesoscale eddy kinetic energy trends of only ~1–3% per decade[28,40], the magnitude of the observed increase in NIC speed and energy is substantial.

The observed intensification of surface NICs has broad implications for Lagrangian transport in the upper ocean. Stronger NICs promote more pronounced near-inertial trajectories and increased trajectory widths, substantially altering the

dispersion of floating materials such as oil spills, marine debris, and biological tracers, with direct consequences for drift prediction and material transport pathways. At the same time, enhanced NICs can increase energy dissipation in the upper ocean, potentially contributing to mixed-layer deepening and sea surface temperature cooling. Beyond the surface layer, near-inertial motions generated within the mixed layer can radiate downward as near-inertial internal waves, providing a key pathway for transferring wind energy into the ocean interior. The documented increase in near-inertial energy therefore implies an enhanced supply of mechanical energy to the deep ocean, with potential consequences for sustaining diapycnal mixing and global overturning circulation. However, whether the current generation of climate models can capture the magnitude and trends of NICs and their impacts on ocean mixing remains uncertain, underscoring the need for improved model representation through enhanced temporal resolution and the development of physically based parameterizations for near-inertial processes.

Methods

Datasets

We use surface current observations from the Global Drifter Program maintained by the Atlantic Oceanographic and Meteorological Laboratory to estimate near-inertial velocities in the upper ocean. The Global Drifter Program provides hourly estimates of location and surface velocity derived from in situ drifter observations[41]. Each drifter is equipped with a subsurface drogue centered at a nominal depth of 15 m, designed to ensure that the measured velocity is representative of the near-surface ocean flow. The Global Drifter Program data used in this study is version 2.01, spanning from 1987 to 2022 and containing 19 396 individual surface drifter trajectories, providing broad spatial coverage across the global ocean. However, because the global drifter array did not reach sufficiently dense coverage until the early 2000s (**Supplementary Fig. 1**), we focus our analysis of NIC variability on the period after 2003, when drifter sampling becomes adequate for robust estimation of long-term changes.

To quantify wind forcing, we employ two state-of-the-art hourly reanalysis wind products. The first is the European Centre for Medium-Range Weather Forecasts Reanalysis v5 (ERA5), which has a spatial resolution of 0.25°[42]. The second is the Climate Forecast System (CFS) reanalysis produced by the National Centers for Environmental Prediction[43,44]. Using two independent wind products allows us to assess the robustness of the estimated near-inertial wind forcing and to reduce potential uncertainties associated with individual reanalysis systems.

MLD information is obtained from an Argo-based observational product (BOA-Argo), which consists of monthly temperature and salinity fields derived from in situ Argo float measurements[45]. This dataset provides MLD estimates based on two commonly used criteria. The first is a density-based criterion, in which the mixed-layer depth H_M is defined as the depth where the potential density referenced to the surface, σ_0, exceeds that at 10 m by a threshold of 0.03 $kg\ m^{-3}$, that is,

$$\sigma_0(z = -H_M) = \sigma_0(z = -10\ \mathrm{m}) + 0.03\ kg\ m^{-3} \quad \ldots\ldots (1)$$

The second criterion defines the MLD as the minimum of density-based and temperature-based estimates, where the temperature-based estimate is given by

$$T(z = -H_M) = T(z = -10\ \mathrm{m}) - 0.2\ ^\circ C \quad \ldots\ldots (2)$$

Both definitions are considered in this study to evaluate the sensitivity of NIC speed estimates to uncertainties in MLD.

Drifter data processing

We first preprocess the surface drifter trajectories to ensure data continuity and quality. Trajectories containing more than 10 consecutive missing values are divided into two independent sub-trajectories; otherwise, missing values are linearly interpolated. Sub-trajectories with durations shorter than 300 hours are subsequently excluded to ensure sufficient temporal coverage for near-inertial analysis.

In general, each drifter is equipped with a subsurface drogue centered at a nominal depth of 15 m. However, as deployment time increases, a fraction of drifters experience drogue loss. Such undrogued drifters can introduce significant observational biases due to enhanced wind drag acting on the surface float[46]. To minimize the influence of wind forcing and drogue loss on the estimated drifter velocities, we apply a wind-driven slip correction[45].

$$\vec{\mathbf{u}} = \vec{\mathbf{u}}_{\mathbf{dr}} - k\vec{\mathbf{u}}_{\mathbf{w}} \quad \ldots\ldots (3)$$

where $\vec{\boldsymbol{u}}_{\boldsymbol{dr}}$ is the drifter velocity, $\vec{\boldsymbol{u}}_{\boldsymbol{w}}$ is the wind velocity linearly interpolated to the position and time of drifter observations, and k is the coefficient of correction. When the drifter is drogued, the coefficient is $k_d = 7 \times 10^{-4}$. When the drifter is undrogued, the coefficient applied is[47,48]:

$$k_u = (\overline{u}_u - \overline{u}_d)/\overline{u}_w + k_d \quad \ldots\ldots \quad (4)$$

where $\overline{u}_d$ and $\overline{u}_u$ represent the downwind components of the drogued and undrogued drifter velocities, respectively, $\overline{u}_w$ is the amplitude of wind speed, and the upper horizontal bar denotes the spatially averaged value in a 2° × 2° spatial box.

After applying the wind-driven slip correction using two independent wind products, the resulting drifter velocity time series are used to extract NICs. Due to the large change of inertial frequency along long drifter trajectories, velocity estimates tracked by a drifter are divided into half-overlapping 300-hour segments in order to extract the near-inertial velocities $\vec{\boldsymbol{u}}_{\boldsymbol{in}}$.[16,20] The near-inertial band $0.75f$–$1.25f$ is adopted, where f is the mean Coriolis frequency of each segment.

Notably, similar spatial patterns of NIC trends are obtained whether using wind-corrected drifter velocities or uncorrected velocities from drogued and undrogued drifters (**Supplementary Fig. 9**). This consistency indicates that the wind correction does not bias the inferred NIC trends, while substantially increasing the number of usable drifter observations.

Near-inertial wind stress and power

To investigate the physical drivers of changes in NICs, we compute near-inertial wind stress (NIWS), which is known to be particularly efficient in exciting NICs through inertial resonance. Accordingly, wind stress is estimated using two complementary

formulations to assess the robustness of the inferred NIWS variability.

In the first approach, wind stress is calculated using only the wind field, without accounting for ocean surface currents,

$$\vec{\boldsymbol{\tau}} = \rho_a C_D \left|\vec{\mathbf{U}}_{\mathbf{10}}\right| \vec{\mathbf{U}}_{\mathbf{10}} \quad \ldots\ldots \quad (5)$$

where ρ_a=1.22 kg m^{-3} is the air density, C_D is the drag coefficient, and $\vec{\mathbf{U}}_{\mathbf{10}}$ is the 10-m wind velocity vector. For ERA5, C_D is provided by ECMWF and accounts for the effects of surface waves, while $\vec{\mathbf{U}}_{\mathbf{10}}$ denotes the 10-m neutral wind velocity vector. For CFS, because 10-m neutral winds are not available, $\vec{\mathbf{U}}_{\mathbf{10}}$ denotes the 10-m true wind velocity vector, and C_D is calculated using the COARE 3.0 bulk algorithm[49]. Wind stresses calculated using (5) are almost identical to the direct wind stress outputs provided by ERA5 and CFS.

In the second approach, the relative motion between the atmosphere and the ocean surface is explicitly considered by incorporating the surface current velocity observed by the drifters,

$$\vec{\boldsymbol{\tau}} = \rho_a C_D \left|\vec{\mathbf{U}}_{\mathbf{10}} - \vec{\mathbf{u}}\right| \left(\vec{\mathbf{U}}_{\mathbf{10}} - \vec{\mathbf{u}}\right) \quad \ldots\ldots \quad (6)$$

where $\vec{\boldsymbol{u}}$ denotes the surface ocean current velocity. Each approach has distinct advantages and limitations. The first method relies on gridded wind products and avoids potential sampling biases associated with the spatiotemporal distribution of surface drifters. The second method interpolates wind velocities to the time and location of individual drifter observations; although this may introduce sampling-related uncertainties, it accounts for the effect of surface currents on air–sea momentum exchange. An error assessment based on HYCOM surface ocean currents driven by CFS winds shows that neglecting surface currents in the wind stress calculation introduces an error of approximately 3% in the estimated NIWS. When surface currents are included, NIWS estimates based on drifter-sampled data reproduce the spatial patterns of both the mean state and trends derived from the gridded data (**Supplementary Fig. 10**).

Following a procedure analogous to the extraction of NICs, a band-pass filter spanning 0.75*f*–1.25*f* is applied separately to the zonal and meridional components of the wind stress, yielding the NIWS components $\tau_{xin}$and τ_{yin}. The magnitude of NIWS is then defined as

$$NIWS = \sqrt{\tau_{xin}^2 + \tau_{yin}^2} \quad \ldots\ldots \quad (7)$$

In addition to NIWS, we also compute near-inertial wind power (NIWP), which directly quantifies the rate at which wind transfers energy to NICs and therefore provides an energetic measure of wind forcing on near-inertial variability. NIWP is defined as

$$NIWP = \vec{\boldsymbol{\tau}} \cdot \vec{\mathbf{u}}_{\mathbf{in}} \quad \ldots\ldots \quad (8)$$

where $\vec{\mathbf{u}}_{\mathbf{in}}$ is the ocean surface near-inertial velocities.

Trend analysis

Owing to the spatiotemporally inhomogeneous distribution of surface drifters, we adopt multiple approaches to estimate trends in NIC speed in order to obtain robust results. As described above, wind-driven slip correction using two independent wind products yields two corresponding sets of drifter velocity estimates. For each velocity dataset, we quantify NIC speed trends using three complementary methods. The first method estimates change as the difference between the mean NIC speed over the last decade (2013–2022) and that over the first decade (2003–2012). The second and third methods compute trends by first constructing gridded annual-mean and gridded monthly-mean NIC speed, respectively, followed by least-squares linear regression to estimate trends and their standard errors.

Quality control is applied to the trend estimates derived from each method. For the first method, trend values are shown only for grid cells with more than 3,000 samples in both decades. For the second method, only grid cells with at least 12 data points per year and data coverage exceeding 15 years are retained. For the third method, grid cells are required to have data coverage exceeding 72 months. Statistical significance is assessed using a criterion in which the magnitude of the estimated trend exceeds one standard error[50]. For the second and third methods, only grid cells that satisfy both the sampling requirements and the significance criterion are displayed. As shown in **Supplementary Fig. 11**, trend estimates derived from the different methods exhibit highly consistent spatial patterns, indicating that the inferred NIC trends are robust to the choice of estimation method.

When computing regional-mean trends, we depart from the approach outlined above by including all grid cells that satisfy the sampling requirements, rather than restricting the calculation to statistically significant grid cells only. Restricting the analysis to significant grid cells alone tends to inflate trend magnitudes, as regions exhibiting weak or negligible changes are excluded, potentially leading to biased estimates. Accordingly, the NIC and NIWS trends reported in the main text represent the average across multiple trend estimation methods, while the associated standard errors are taken as the mean of those derived from the second and third methods. For NIWP, which is proportional to the product of NIWS and NIC, the use of the second and third methods substantially amplifies the effects of spatially inhomogeneous drifter sampling, leading to large uncertainties. To avoid this sampling-induced bias, NIWP is therefore estimated exclusively using the first method.

Slab model simulations

Slab models are widely used to simulate wind-driven near-inertial motions in the ocean mixed layer[12,17,36]. To quantify the contribution of long-term changes in MLD to trends in NIC speed, we conduct slab-model simulations forced by two independent wind products (ERA5 and CFS). The governing equations of the slab model are

$$\begin{cases} \dfrac{\partial u}{\partial t} + ru - fv = \dfrac{\tau_x}{\rho_0 H_M} \\ \dfrac{\partial v}{\partial t} + rv + fu = \dfrac{\tau_y}{\rho_0 H_M} \end{cases} \quad \cdots\cdots (9)$$

where u and v are the zonal and meridional components of the mixed-layer velocity, respectively; ρ_0 is the reference seawater density; $\vec{\boldsymbol{\tau}} = (\tau_x, \tau_y)$ denotes the wind stress; and H_M is the mixed-layer depth. The parameter r represents a linear damping term that parameterizes the loss of near-inertial energy from the mixed layer t o

t To isolate the influence of long-term MLD changes, we perform paired si mulations in which the wind forcing is held identical while the MLD differs. One set of simulations uses the climatological monthly mean MLD field that retains only the seasonal cycle, whereas the other uses the observed monthly MLD, including both seasonal and long-term variations. The difference between these two simulations allows us to quantify the relative contribution of long-term MLD changes to trends in NIC speed.

a It should be noted that the slab model assumes vertically uniform mixed-layer velocity and idealizes damping and downward energy radiation. It therefore cannot fully represent vertical shear, subsurface stratification, mesoscale vorticity, or other three-dimensional processes affecting NIC amplitude and trends. However, its simplicity enables individual physical effects to be isolated through controlled sensitivity experiments. We therefore use it primarily to quantify the contribution of MLD variations, which have been suggested to modulate NIC strength[17, 34], rather than to reproduce the full observed trend magnitude.

i o r .

W e

a d o p t

▮

=

0 . 2 5

P A G E

$10^{-5}s^{-1}$, a value that yields slab-model NIC speed close to the drifter-based observations. NICs are extracted from the model output using the same band-pass filter spanning

Data availability

The Global Drifter Program data are provided by Atlantic Oceanographic and Meteorological Laboratory, available at www.aoml.noaa.gov/phod/gdp/hourly_data.php. ERA5 wind data is provided by ECMWF, downloaded from https://cds.climate.copernicus.eu/cdsapp#!/dataset/reanalysis-era5-single-levels?tab=form. CSFv2 wind data are obtained from the U. S. Global Ocean Data Assimilation Experiment website https://www.hycom.org/dataserver/ncep-cfsr and www.hycom.org/dataserver/ncep-cfsv2. BOA-Argo mixed layer depth data are available at https://argo.ucsd.edu/data/argo-data-products/. HYCOM current data are downloaded from https://www.hycom.org/dataserver/gofs-3pt1/reanalysis and https://www.hycom.org/dataserver/gofs-3pt1/analysis. Land boundaries are obtained from Natural Earth (https://www.naturalearthdata.com/downloads/50m-physical-vectors). The processed datasets generated in this study are available from Zenodo at https://doi.org/10.5281/zenodo.18607058.

Code availability

All figures were generated by the authors using MATLAB and m_map toolbox. Code link to reproduce the results: https://doi.org/10.5281/zenodo.18607058

Funding

This study is supported by the National Natural Science Foundation of China (42430401, 42276026), Guangdong Basic and Applied Basic Research Foundation (2023A1515012691), the Chinese Academy of Sciences (SCSIO202204), and the Open Project Program of State Key Laboratory of Tropical Oceanography (LTOZZ2203).

Author contributions

Y.Z., X.Z., and Y.D. conceived this study. Y.Z. wrote the initial manuscript and performed the analyses in discussion with X.Z, D.S, W.W., H.G., and Y.D. All authors contributed to interpreting results, discussion, and improvement of this paper.

Competing interests

The authors declare no competing interests.

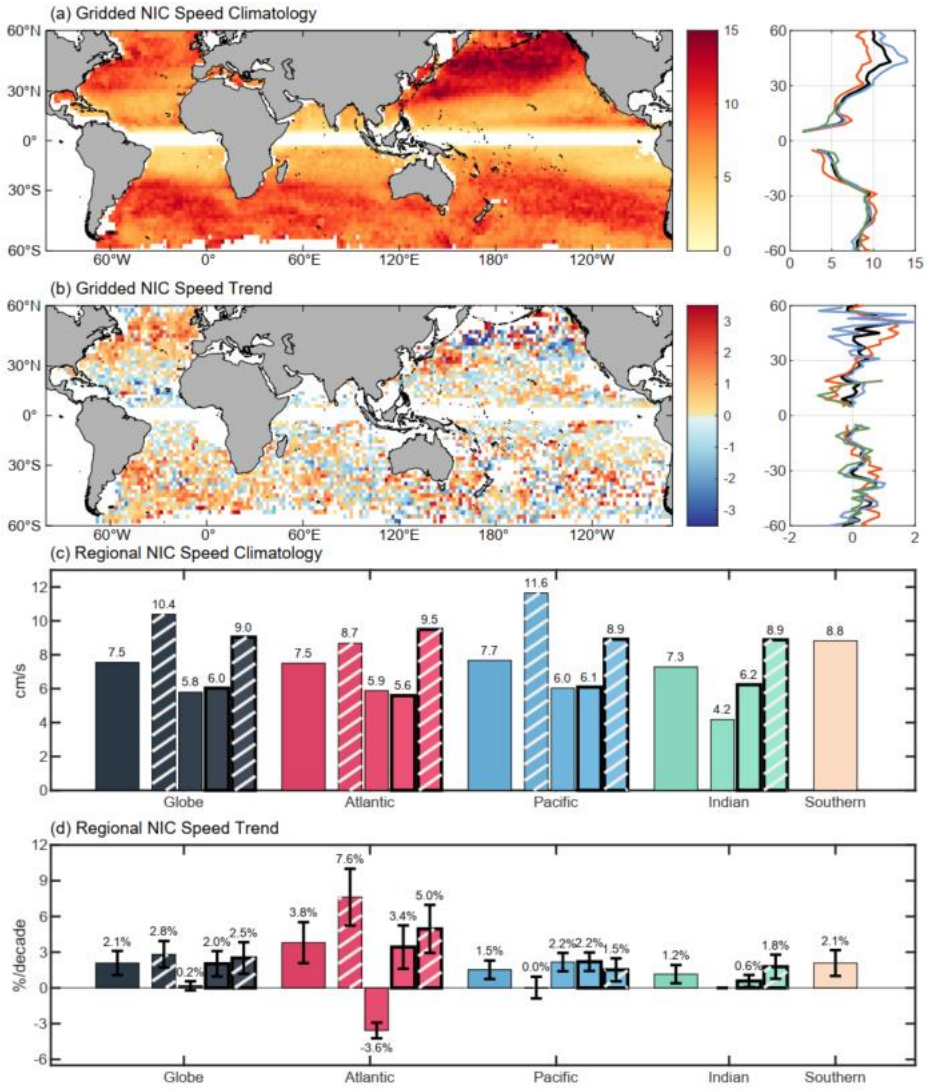


Fig. 1| Global climatology and trends of near-inertial currents (NICs) derived from surface drifter observations. a Gridded climatology of NIC speed (cm s^{-1}) and its zonal-mean distribution for different ocean basins. **b** Linear trend of gridded NIC speed (cm s^{-1} $decade^{-1}$) and its zonal-mean values for different ocean basins. Regions with insufficient drifter sampling or without a significant trend (see Methods) are shown in white. In panels **a** and **b**, the black, red, blue, and green curves on the right denote the zonal averages for the global ocean, Atlantic, Pacific, and Indian Oceans, respectively. **c** Regional NIC speed climatology summarized for major basins. **d** Regional trends expressed as percent changes in NIC speed across the global ocean and individual basins. Error bars indicate one standard error. Black, red, blue, green, and yellow bars in (**c-d**) represent the global ocean, Atlantic, Pacific, Indian, and Southern oceans, respectively. For each basin, the leftmost bar indicates the full-latitude mean. From left to right, the remaining adjacent bars (striped–no outline, unstriped–no outline, unstriped–outlined, striped–outlined) correspond to the high latitudes of the Northern Hemisphere (30–60°N), low latitudes of the Northern Hemisphere (5–30°N), low latitudes of the Southern Hemisphere (5–30°S), and high latitudes of the Southern Hemisphere (30–60°S).

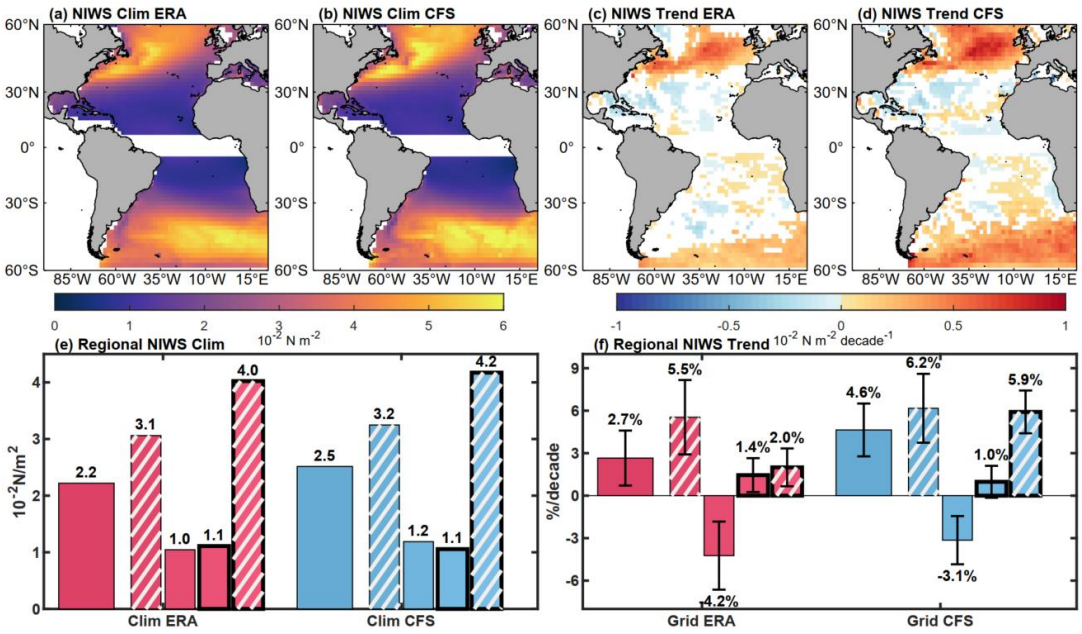


Fig. 2| Near-inertial wind stress (NIWS) climatology and trends in the Atlantic Ocean derived from ERA5 and CFS. a–b, Gridded NIWS climatology in the Atlantic Ocean derived from ERA5 (**a**) and CFS (**b**) reanalysis data. **c–d**, Linear trends in gridded NIWS from ERA5 (**c**) and CFS (**d**). Regions without a significant trend are shown in white. **e**, Regional NIWS climatology in the Atlantic Ocean. **f**, Regional NIWS trends expressed as percent changes across the Atlantic Ocean. Error bars indicate one standard error. In panels **e** and **f**, red and blue bars represent results from ERA5 and CFS, respectively. For each wind product, the leftmost bar denotes the full-Atlantic mean. From left to right, the remaining adjacent bars (striped–no outline, unstriped–no outline, unstriped–outlined, striped–outlined) correspond to the high latitudes of the North Atlantic (30–60°N), low latitudes of the North Atlantic (5–30°N), low latitudes of the South Atlantic (5–30°S), and high latitudes of the South Atlantic (30–60°S).

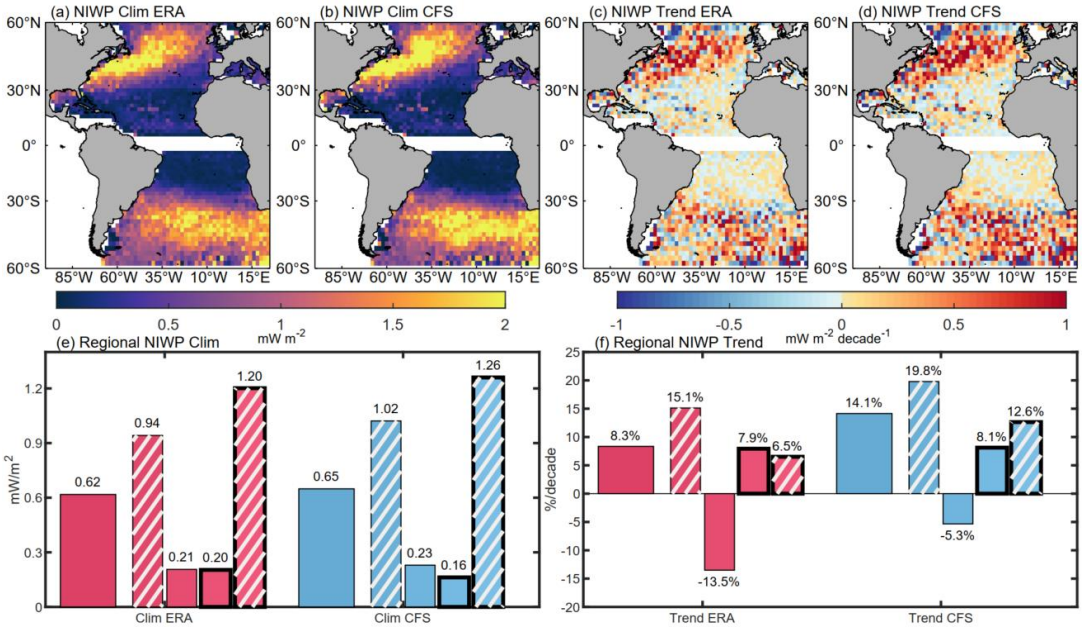


Fig. 3| Near-inertial wind power (NIWP) climatology and trends in the Atlantic Ocean derived from ERA5 and CFS. a–b, Gridded NIWP climatology in the Atlantic Ocean derived from ERA5 (**a**) and CFS (**b**) data. **c–d**, Trends in gridded NIWP from ERA5 (**c**) and CFS (**d**). **e**, Regional NIWP climatology in the Atlantic Ocean. **f**, Regional NIWS trends expressed as percent changes across the Atlantic Ocean. In panels **e** and **f**, red and blue bars represent results from ERA5 and CFS, respectively. For each wind product, the leftmost bar denotes the full-Atlantic mean. From left to right, the remaining adjacent bars (striped–no outline, unstriped–no outline, unstriped–outlined, striped–outlined) correspond to the high latitudes of the North Atlantic (30–60°N), low latitudes of the North Atlantic (5–30°N), low latitudes of the South Atlantic (5–30°S), and high latitudes of the South Atlantic (30–60°S).

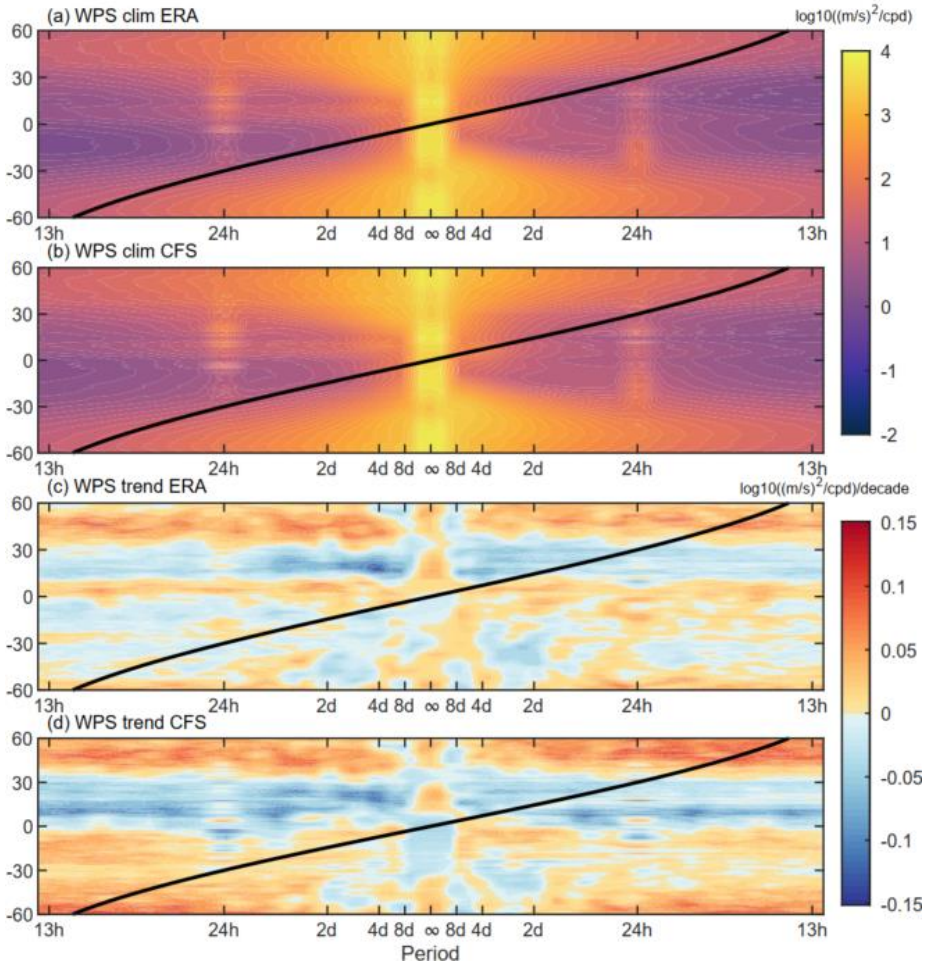


Fig. 4| Wind power rotary spectrum climatology and trends in the Atlantic Ocean derived from ERA5 and CFS. a–b, Climatological wind power rotary spectra in the Atlantic Ocean derived from ERA5 (**a**) and CFS (**b**). **c–d**, Trends in the wind power rotary spectra derived from ERA5 (**c**) and CFS (**d**). In panels **a–d**, the horizontal axis denotes the spectral period, with clockwise and counterclockwise rotary components shown on the right and left sides of the x-axis, respectively. The black curves indicate the inertial frequency corresponding to each latitude.

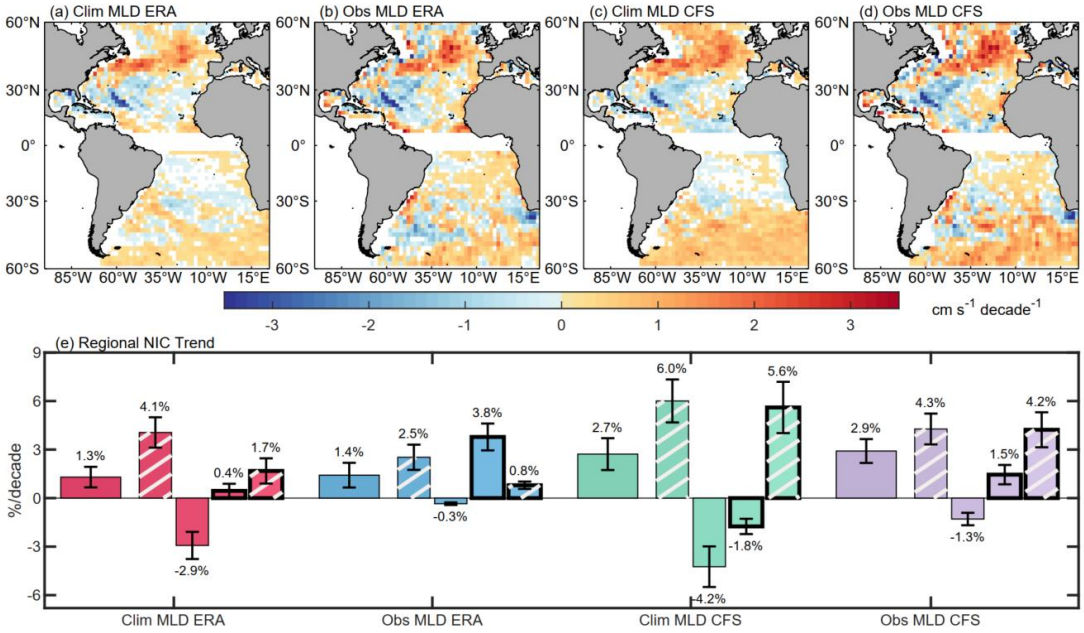


Fig. 5| Influence of mixed-layer depth (MLD) representation in slab-model simulations on the trend of near-inertial currents (NICs) in the Atlantic Ocean. **a–b**, Trends in Atlantic NIC speed simulated using ERA5 wind forcing combined with a purely seasonal MLD climatology (**a**) and the observed monthly MLD (**b**). **c–d**, Same as panels **a–b**, but for simulations driven by CFS wind forcing with a seasonal MLD (**c**) and a full monthly MLD (**d**). **e**, Regional NIC speed trends expressed as percent changes across the Atlantic Ocean. Error bars indicate one standard error. Red, blue, green, and purple bars represent results obtained from the four simulations shown in panels a–d, respectively. For each simulation, the leftmost bar denotes the full-Atlantic mean. From left to right, the remaining adjacent bars (striped–no outline, unstriped–no outline, unstriped–outlined, striped–outlined) correspond to the high latitudes of the North Atlantic (30–60°N), low latitudes of the North Atlantic (5–30°N), low latitudes of the South Atlantic (5–30°S), and high latitudes of the South Atlantic (30–60°S).

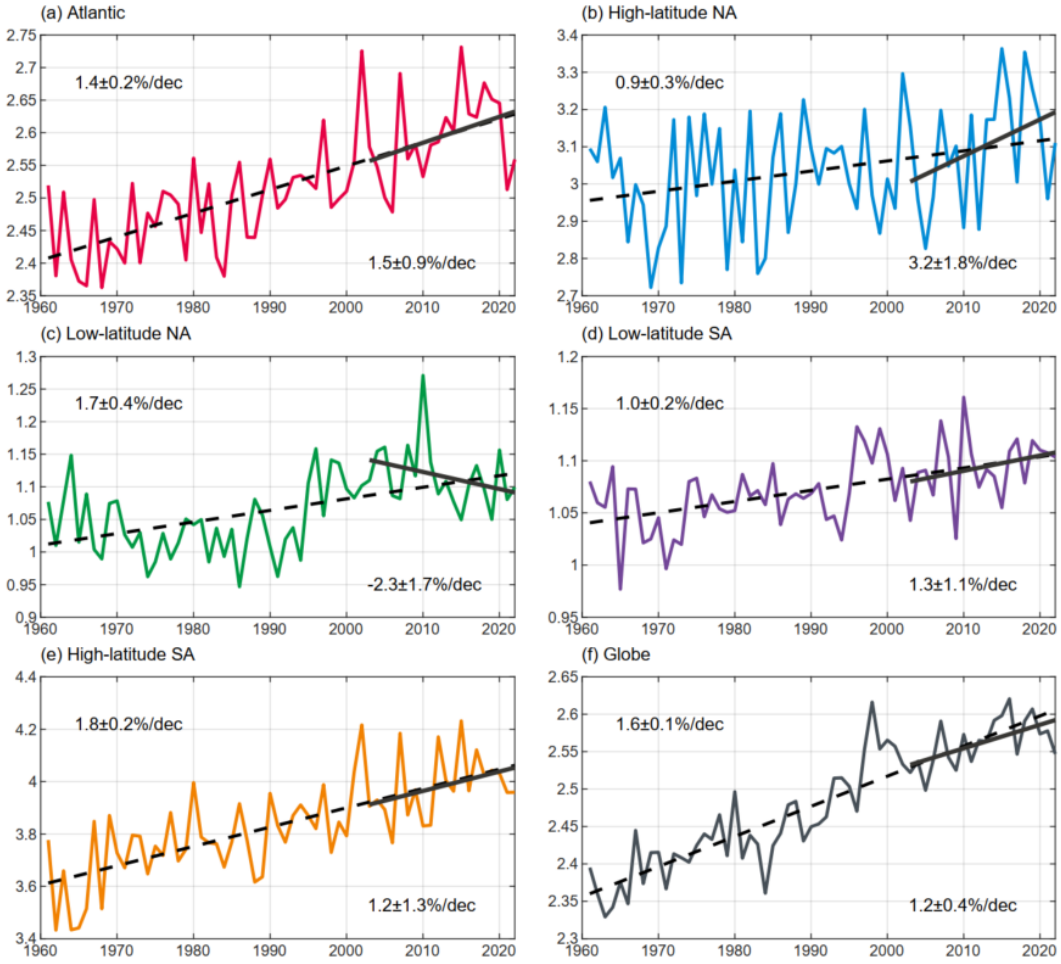


Fig. 6| Time series and trends of near-inertial wind stress (NIWS) from 1961 to 2022 derived from ERA5. Panels **a–f** show regionally averaged NIWS values (units: 10^{-2} N m^{-2}) for the Atlantic Ocean (**a**), high-latitude North Atlantic (**b**), low-latitude North Atlantic (**c**), low-latitude South Atlantic (**d**), high-latitude South Atlantic (**e**), and the global ocean (**f**), respectively. The black dashed lines denote linear trends over 1961–2022, with the corresponding percentage changes indicated in the upper-left corner of each panel. The gray solid lines represent trends over 2003–2022, with percentage changes shown in the lower-right corner of each panel.

References

1 Falkowski, P., Barber, R. & Smetacek, V. Biogeochemical controls and feedbacks on ocean primary production. Science **281**, 200-206 (1998). https://doi.org:10.1126/science.281.5374.200

2 Wunsch, C. Vertical Mixing, Energy, and the General Circulation of the Oceans. Annual Review of Fluid Mechanics **36**, 281-314 (2004). https://doi.org:10.1146/annurev.fluid.36.050802.122121

3 Marshall, J. & Speer, K. Closure of the meridional overturning circulation through Southern Ocean upwelling. Nature Geoscience **5**, 171-180 (2012). https://doi.org:10.1038/ngeo1391

4 Talley, L. Closure of the Global Overturning Circulation Through the Indian, Pacific, and Southern Oceans: Schematics and Transports. Oceanography **26**, 80-97 (2013). https://doi.org:10.5670/oceanog.2013.07

5 Gruber, N., Clement, D., Carter, B. R., Feely, R. A. & van Heuven, S. The oceanic sink for anthropogenic CO2 from 1994 to 2007. Science **363**, 1193-+ (2019). https://doi.org:10.1126/science.aau5153

6 Pollard, R. & Millard, R. Comparison between Observed and Simulated Wind-Generated Inertial Oscillations. Deep-Sea Research **17**, 813-& (1970). https://doi.org:10.1016/0011-7471(70)90043-4

7 D'asaro, E. The Energy Flux from tthe Wind to Near-Inertial Motions in The Surface Mixed Layer. Journal Of Physical Oceanography **15**, 1043-1059 (1985). https://doi.org:10.1175/1520-0485(1985)015<1043:TEFFTW>2.0.CO;2

8 Thomson, R. E., LeBlond, P. H. & Rabinovich, A. B. Satellite‐tracked drifter measurement of inertial and semidiurnal currents in the northeast Pacific. Journal of Geophysical Research: Oceans **103**, 1039-1052 (1998). https://doi.org:10.1029/97jc02374

9 Alford, M. H., MacKinnon, J. A., Simmons, H. L. & Nash, J. D. Near-Inertial Internal Gravity Waves in the Ocean. Annual Review of Marine Science 8, 95-123 (2016). https://doi.org:10.1146/annurev-marine-010814-015746

10 Alford, M. Internal swell generation: The spatial distribution of energy flux from the wind to mixed layer near-inertial motions. Journal of Physical Oceanography **31**, 2359-2368 (2001). https://doi.org:10.1175/1520-0485(2001)031<2359:ISGTSD>2.0.CO;2

11 Watanabe, M. & Hibiya, T. Global estimates of the wind‐induced energy flux to inertial motions in the surface mixed layer. Geophysical Research Letters **29** (2002). https://doi.org:10.1029/2001gl014422

12 Alford, M. H. Improved global maps and 54‐year history of wind‐work on ocean inertial motions. Geophysical Research Letters **30** (2003). https://doi.org:10.1029/2002gl016614

13 Jiang, J., Lu, Y. & Perrie, W. Estimating the energy flux from the wind to ocean inertial motions: The sensitivity to surface wind fields. Geophysical Research Letters **32** (2005). https://doi.org:10.1029/2005gl023289

14 Furuichi, N., Hibiya, T. & Niwa, Y. Model‐predicted distribution of wind‐induced internal wave energy in the world's oceans. Journal of Geophysical Research: Oceans **113** (2008). https://doi.org:10.1029/2008jc004768

15 Rimac, A., von Storch, J. S., Eden, C. & Haak, H. The influence of high‐resolution wind stress field on the power input to near‐inertial motions in the ocean. Geophysical Research Letters **40**, 4882-4886 (2013). https://doi.org:10.1002/grl.50929
16 Liu, Y., Jing, Z. & Wu, L. Wind Power on Oceanic Near‐Inertial Oscillations in the Global Ocean Estimated From Surface Drifters. Geophysical Research Letters **46**, 2647-2653 (2019). https://doi.org:10.1029/2018gl081712
17 Alford, M. H. Revisiting Near-Inertial Wind Work: Slab Models, Relative Stress, and Mixed Layer Deepening. Journal of Physical Oceanography **50**, 3141-3156 (2020). https://doi.org:10.1175/jpo-d-20-0105.1
18 Li, X., Li, C., Yang, Z. & Pichel, W. SAR imaging of ocean surface oil seep trajectories induced by near inertial oscillation. Remote Sensing of Environment **130**, 182-187 (2013). https://doi.org:10.1016/j.rse.2012.11.019
19 Lumpkin, R., Ozgokmen, T. & Centurioni, L. Advances in the Application of Surface Drifters. Annual Review of Marine Science **9**, 59-81 (2017). https://doi.org:10.1146/annurev-marine-010816-060641
20 Zheng, Y., Wu, W., Wang, M., Zhang, Y. & Du, Y. Different trajectory patterns of ocean surface drifters modulated by near-inertial oscillations. Environmental Research Letters **19** (2024). https://doi.org:10.1088/1748-9326/ad7745
21 Price, J. Internal Wave Wake of a Moving Storm .1. Scales, Energy Budget and Observations. Journal of Physical Oceanography **13**, 949-965 (1983). https://doi.org:10.1175/1520-0485(1983)013<0949:IWWOAM>2.0.CO;2
22 Gill, A. On the Behavior of Internal Waves in The Wakes of Storms. Journal of Physical Oceanography **14**, 1129-1151 (1984). https://doi.org:10.1175/1520-0485(1984)014<1129:OTBOIW>2.0.CO;2
23 Zhai, X., Greatbatch, R. J. & Zhao, J. Enhanced vertical propagation of storm‐induced near‐inertial energy in an eddying ocean channel model. Geophysical Research Letters **32** (2005). https://doi.org:10.1029/2005gl023643
24 Alford, M. H., Cronin, M. F. & Klymak, J. M. Annual Cycle and Depth Penetration of Wind-Generated Near-Inertial Internal Waves at Ocean Station Papa in the Northeast Pacific. Journal of Physical Oceanography **42**, 889-909 (2012). https://doi.org:10.1175/jpo-d-11-092.1
25 Chen, Z. et al. Downward Propagation and Trapping of Near-Inertial Waves by a Westward-Moving Anticyclonic Eddy in the Subtropical Northwestern Pacific Ocean. Journal of Physical Oceanography **53**, 2105-2120 (2023). https://doi.org:10.1175/jpo-d-22-0226.1
26 Yang, H. et al. Intensification and poleward shift of subtropical western boundary currents in a warming climate. Journal of Geophysical Research: Oceans **121**, 4928-4945 (2016). https://doi.org:10.1002/2015jc011513
27 Hu, S. et al. Deep-reaching acceleration of global mean ocean circulation over the past two decades. Science Advances **6** (2020). https://doi.org:10.1126/sciadv.aax7727
2
8
29 Meng, Q. et al. Surface warming‐induced global acceleration of upper ocean currents.
a
r
t
nez-Moreno, J. et al. Global changes in oceanic mesoscale currents over the satellite altimetry record. Nature Climate Change **11**, 397-403 (2021).

Science Advances **8** (2022). https://doi.org:10.1126/sciadv.abj8394
30 Wang, S. et al. A more quiescent deep ocean under global warming. Nature Climate Change **14**, 961-967 (2024). https://doi.org:10.1038/s41558-024-02075-2
31 Yang, Z. et al. Enhanced generation of internal tides under global warming. Nature Communications **15**, 7657 (2024). https://doi.org:10.1038/s41467-024-52073-3
32 Yang, H. et al. Onshore intensification of subtropical western boundary currents in a warming climate. Nature Climate Change **15**, 301-307 (2025). https://doi.org:10.1038/s41558-025-02258-5
33 Gong, Y. et al. Accelerated internal tides in a warming climate. Science advances **11** (2025). https://doi.org:10.1126/sciadv.adq4577
34 Qian, J., Zhai, X., Wang, Z. & Jochum, M. Distribution and Trend of Wind Power Input to Near‐Inertial Motions in the Southern Ocean. Geophysical Research Letters **50** (2023). https://doi.org:10.1029/2023gl105411
35 Ma, Y. et al. Fewer tropical cyclones yield more near-inertial wind work to the global ocean over the past four decades. Environmental Research Letters **19** (2024). https://doi.org:10.1088/1748-9326/ad5854
36 Zhai, X. Latitudinal Dependence of Wind-Induced Near-Inertial Energy. Journal of Physical Oceanography **45**, 3025-3032 (2015). https://doi.org:10.1175/jpo-d-15-0166.1
37 Lin, X., Zhai, X., Wang, Z. & Munday, D. R. Mean, Variability, and Trend of Southern Ocean Wind Stress: Role of Wind Fluctuations. Journal of Climate **31**, 3557-3573 (2018). https://doi.org:10.1175/jcli-d-17-0481.1
38 Conn, S., Fitzgerald, J. & Callies, J. Interpreting Observed Interactions between Near-Inertial Waves and Mesoscale Eddies. *Journal of Physical Oceanography* **54**, 485-502 (2024). https://doi.org:10.1175/jpo-d-23-0139.1
39 Huang, H. et al. Contrasting Responses of Atlantic and Pacific Tropical Cyclone Activity to Atlantic Multidecadal Variability. Geophysical Research Letters 50 (2023). https://doi.org:10.1029/2023gl102959
40 Barcelo-Llull, B. et al. Kuroshio Extension and Gulf Stream dominate the Eddy Kinetic Energy intensification observed in the global ocean. Scientific Reports **15**, 21754 (2025). https://doi.org:10.1038/s41598-025-06149-9
41 Elipot, S. et al. A global surface drifter data set at hourly resolution. Journal of Geophysical Research: Oceans **121**, 2937-2966 (2016). https://doi.org:10.1002/2016jc011716
42 Hersbach, H. et al. The ERA5 global reanalysis. Quarterly Journal of the Royal Meteorological Society **146**, 1999-2049 (2020). https://doi.org:10.1002/qj.3803
43 Saha, S. et al. The NCEP Climate Forecast System Reanalysis. Bulletin of the American Meteorological Society **91**, 1015-1058 (2010). https://doi.org:10.1175/2010bams3001.1
44 Saha, S. et al. The NCEP Climate Forecast System Version 2. Journal of Climate **27**, 2185-2208 (2014). https://doi.org:10.1175/jcli-d-12-00823.1
45 Li, H. et al. Development of a global gridded Argo data set with Barnes successive corrections. Journal of Geophysical Research: Oceans **122**, 866-889 (2017). https://doi.org:10.1002/2016jc012285
46 Laurindo, L. C., Mariano, A. J. & Lumpkin, R. An improved near-surface velocity climatology for the global ocean from drifter observations. Deep Sea Research Part I: Oceanographic Research Papers **124**, 73-92 (2017).

https://doi.org:10.1016/j.dsr.2017.04.009

47 Pazan, S. E. & Niiler, P. P. Recovery of near-surface velocity from undrogued drifters. Journal of Atmospheric and Oceanic Technology **18**, 476-489 (2001). https://doi.org:10.1175/1520-0426(2001)018<0476:RONSVF>2.0.CO;2

48 Niiler, P. P. & Paduan, J. D. Wind-driven motions in the northeast Pacific as measured by lagrangian drifters. Journal of Physical Oceanography **25**, 2819-2830 (1995). https://doi.org:10.1175/1520-0485(1995)025<2819:WDMITN>2.0.CO;2

49 Fairall, C. W., Bradley, E. F., Hare, J. E., Grachev, A. A. & Edson, J. B. Bulk Parameterization of Air–Sea Fluxes: Updates and Verification for the COARE Algorithm. *Journal of Climate* **16**, 571-591 (2003). https://doi.org:10.1175/1520-0442(2003)016<0571:bpoasf>2.0.co;2

50 Sallee, J. B. et al. Summertime increases in upper-ocean stratification and mixed-layer depth. Nature **591**, 592-598 (2021). https://doi.org:10.1038/s41586-021-03303-x